Radiographic simulation and validation studies on weld joints of annular tanks and cylindrical tanks

IOP Conf. Series: Materials Science and Engineering **554** (2019) 012008 doi:10.1088/1757-899X/554/1/012008

Radiographic simulation and validation studies on weld joints of annular tanks and cylindrical tanks

Kumar, S.*, Menaka, M., and Venkatraman, B.

Health, Safety and Environmental Group, Indira Gandhi Centre for Atomic Research (IGCAR), Kalpakkam 603 102, Tamil Nadu, India.

Corresponding author, email: kumar257selvam@gmail.com

Abstract. The application of the radiographic simulation studies on the weld joints in nuclear fuel reprocessing tanks used for optimization of radiographic testing parameters. In the nuclear reprocessing plant, Annular and cylindrical tanks are used to store the reprocessed solution of the spent fuel pins from the reactor. These annular and cylindrical tanks were installed 15 years ago. AERB (Atomic Energy Regulatory Board) has requested for requalification of these tanks before commissioning. As part of the requalification of tanks, the volumetric NDE techniques were proposed to be used for evaluation of the weld joints in the tanks. Before carrying out the radiographic examination on the actual tanks, computer simulation of radiography was studied on standard weld pad. Radiographic simulation is utilized for various purposes in NDT. This radiographic diagnostic model utilized for study about incorporates a description of the radiation source, the interaction of radiation with test pieces and defects, and the detection process. The modeling results were validated with radiographic inspection carried out with weld pad sample of 6mm thickness. The error percentage in the optical density achieved between simulation and experiment radiographic inspection was ± 5%. Hence the optimization parameters using simulation for the weld pad helps to reduce the number of exposures, inspection time and increase defect detectability of the inspection.

1. Introduction

CORAL (COmpact Reprocessing facility for Advanced fuels in Lead shielded cell) is the pilot plant successfully demonstrated by reprocessing spent fuels from Fast Breeder Test Reactor (FBTR). Based on the feedback obtained from CORAL operations, a demonstration fuel reprocessing plant of still higher capacity has been designed and constructed. The main objectives of this plant are to reprocess the fuel of FBTR on regular basis and that of PFBR (Prototype Fast Breeder Reactor) on experimental basis [1-3]. In this plant, cylindrical and annular tanks are used to store the process solution of the spent fuel pins from the reactor. Tanks were erected 15 years ago. AERB (Atomic Energy Regulatory Board) has requested for the requalification of these tanks before commissioning. Based on AERB requirements, requalification methodology for process vessels and associated pipings erected at various cells of Demonstration Fast Reactor Fuel Reprocessing Plant (DFRP) has been planned. A sampling percentage of around 10 % covering entire spectrum of process vessels will be covered for requalification. Selection of critical process vessels to be covered in the sampling plan was decided by the designer based upon criticality, process conditions and accessibility. As part of the requalification of tanks, the volumetric NDE techniques [4] were proposed to be used for evaluation of weld joints in the tanks. Before carrying out radiographic examination on the actual tanks, computer simulation of radiography [5-7] was studied on standard weld samples in *aRTist* (Analytical Radiography Testing

Inspection Simulation Tool) software. The modelling results were validated with experimental results of weld pad samples. After that radiographic simulation was carried on actual tanks. Then optimizing the parameters was used in radiographic examination on actual tanks [8]. aRTist simulation programming is created by BAM (Federal Institute of Materials Research and Testing), Germany [9]. It consolidates diagnostic modeling of the RT inspection process with CAD oriented object description. This product tool for numerical simulation is displayed which creates practical radiographs on the premise of virtual part portrayals and very much characterized radiological parameters. This simulation tool satisfies the practical industrial requirements and connected for inspection planning. This simulation program utilizes an analytical procedure model, productive ray tracing algorithms, industry standard boundary portrayals, and a graphical UI with 3D perception to meet these requirements. This simulation procedure can be subdivided into three autonomous parts: the generation of X- ray beam, the interaction between the radiation and material, and the imaging process. The radiation material communication can be portrayed by the Boltzmann transport equation. Ray tracing model based on the attenuation law described the detailed solution of the image.For the interaction of radiation with material we limit our model to photon interactions and do not represent electrons. Appropriately the accompanying interaction mechanisms are viewed as: the photoelectric effect, coherent and incoherent scattering, and for photon energies bigger than 1 MeV pair production.

The photon transport model is using the stationary Boltzmann equation

$$\boldsymbol{\Omega}\cdot\nabla I\left(\boldsymbol{r},E,\boldsymbol{\Omega}\right)+\mu\left(E\right)I\left(\boldsymbol{r},E,\boldsymbol{\Omega}\right)=$$
$$\int_0^\infty \mathrm{d}E'\int_{4\pi}\mathrm{d}\Omega'\;\sigma\left(E'\to E,\boldsymbol{\Omega}'\to\boldsymbol{\Omega}\right)I\left(\boldsymbol{r},E',\boldsymbol{\Omega}'\right)+S\left(\boldsymbol{r},E,\boldsymbol{\Omega}\right)$$

It describes the variation of the photon flux $I(\boldsymbol{r}, E, \Omega)$ at position $\boldsymbol{r}$ with direction Ω and energy E. The reduction of the flux by the interaction of photons with matter given by the linear attenuation coefficient $\mu(E)$ is the left hand side of the equation.

$$\mu\left(E\right)=\tau+\sigma_{\text{coherent}}+\sigma_{\text{incoherent}}+\pi$$

τ is the absorption coefficient, σ_{coherent} and $\sigma_{\text{incoherent}}$ are scattering coefficients and π is the pair production coefficient.The increase of the photon flux $I(\boldsymbol{r}, E, \Omega)$ by scattering contributions from other energies E' and other directions Ω' given by the scattering cross section $\sigma(E'\to E,\Omega'\to\Omega)$ as well as by internal photon sources $S(\boldsymbol{r}, E,\Omega)$ such as X-ray fluorescence or electron-positron annihilation described in right hand side. The right hand side of the equation is vanished by neglecting the scattering contributions. Then ordinary differential equation can be directly incorporated prompting the well known attenuation law

$$I_p\left(\boldsymbol{r},\boldsymbol{\Omega},E\right)=I_0\left(\boldsymbol{r},\boldsymbol{\Omega},E\right)e^{-\int_0^{|r-r_0|}\mathrm{d}R\;\mu\left(\boldsymbol{r}-R\boldsymbol{\Omega},E\right)}$$

The primary photon flux $I_p(\boldsymbol{r}, E, \Omega)$ derived from the initial flux $I_0(\boldsymbol{r}, E, \Omega)$, which conveys the significant data for radiographic methods [11].

1.1. Part geometric model

The input for geometrical model is a triangulated surface model of the test piece in the industry standard STL format. Along these lines it is conceivable to work with arbitrary geometry and to interface straightforwardly with CAD programming. Material types are constantly allocated to the part geometries form an extensible material rundown within the program [9]. Initial modeling studies were carried out

using stainless steel 304L weld pad of 6mm thick with dimension 100mmX100mm. Modelled weld plate in the STL format is shown in Figure 1.

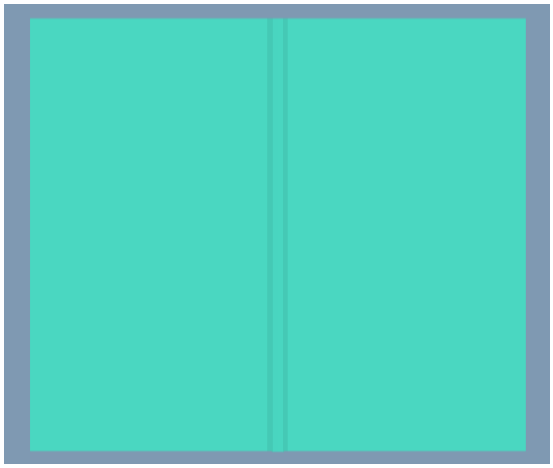

Figure 1. CAD model of weld pad for simulation

1.2. Source model

With respect to X-ray beam generation in the source, aRTist proposes an X-ray tube model, which can be utilized between 30kV to 450kV.For the weld pad radiographic inspection modeling studies, 110kV, 120kV and 130 kV tube voltages were simulated. This executed X-ray tube display simulates the physical marvels engaged with bremsstrahlung and characteristic photon creation with semi-empiric model. It considers the anode angle and composition, the inherent and extra filtration and the photons leave angle. Source modeling was carried out using tungsten target with anode angle 40^{o} and aluminum filter for reduction in beam hardening. The typical energy spectrum of tungsten target for 130KV simulated x-ray source is shown in the Figure 2. The tube current of 4.3mA was fixed for the simulation.

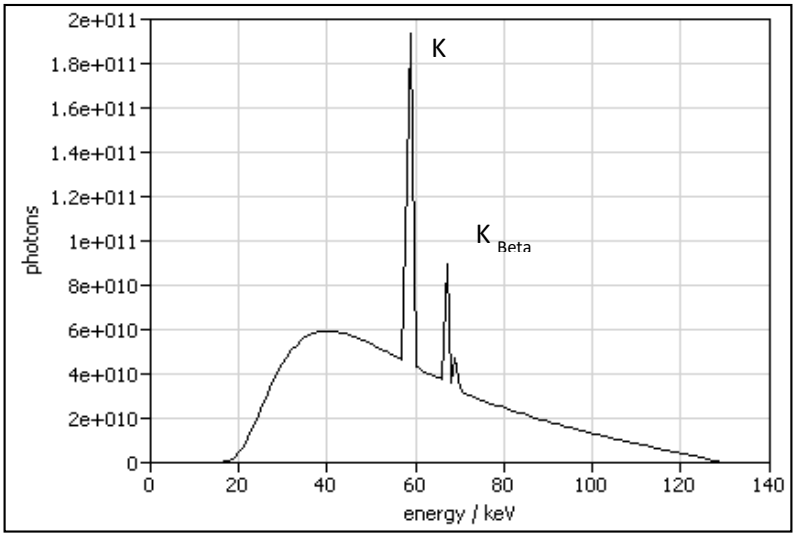

Figure 2. Energy spectra of tungsten target for 130kV

1.3. Detector modelling

Detectors are displayed in two progressive strides. The first, basic to a wide range of detectors registers the energy deposition in the delicate piece of the detector utilizing the energy absorption attenuation coefficients. The second one is particular to each kind of detector which recreates the progressive physical phenomena engaged with the energy to signal change. Different models are adjusted for the different detectors, for example, scintillating screen, saw by CCD camera, photomultiplier and a film [10]. Transmission functions depend on the property of the detectors. [11] For the modeling studies the detectors were D4 film, D5 film, and D7 film with size of 250 X105 mm.

1.4. Virtual set up

The computer simulation models the genuine review situation by characterizing a virtual a setup. Other than radiation source and detector, at least one geometrical part portrayals can be arranged freely in virtual space. Parts are modeled in CAD programming and imported into the aRTist. A cover of the parts characterized in the scene is resolved by their need. This takes into consideration adaptable defect descriptions that are autonomous from the encompassing material. To decide the attenuation of radiation the length of homogeneous material segments on the direct associations amongst source and detector indicated have been computed. Intelligent arrangeable part portrayals can without much of a stretch be overseen in the virtual 3D scene. Cover of geometries in the scene and blend by Boolean operator's prompts variable imperfection descriptions free frame encompassing host material of defect. Inside the program it is conceivable to create geometrical primitives like cuboids, ellipsoids and cylinders. Other part geometries can be given in STL format [12]. Defects such as porosity, lack of penetration, lack of fusion and cracks were embedded in the weld region with varying dimension and orientation for the study. For simulation calculation, a volumetric defect with a size of 2mm at depth 3mm in the weld region was used. In the standard 3D scene of virtual setup, the source to detector can be fixed. To optimize, the source can be moved like any other part in virtual setting. To set it at an exact distance the position may be defined numerically as in this case, it was varied from 1000mm, 800mm, 600mm. A reference point is defined using a red ball which is placed at the centre of the part to help in rotation of the part. The setup has also penetrameter models provided with the program. Figure 3 shows the simulation of radiographic testing in weld pad model with source and detector. Figure 4 shows the parameters used in the radiographic simulation.

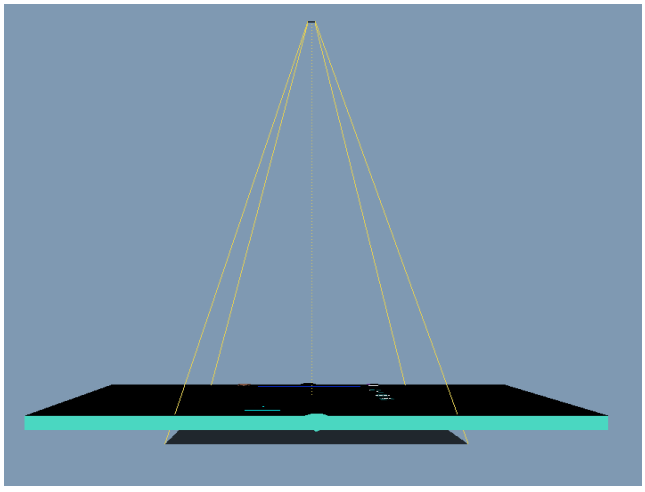

Figure 3. Simulation of Radiographic testing in weld pad model with source and detector

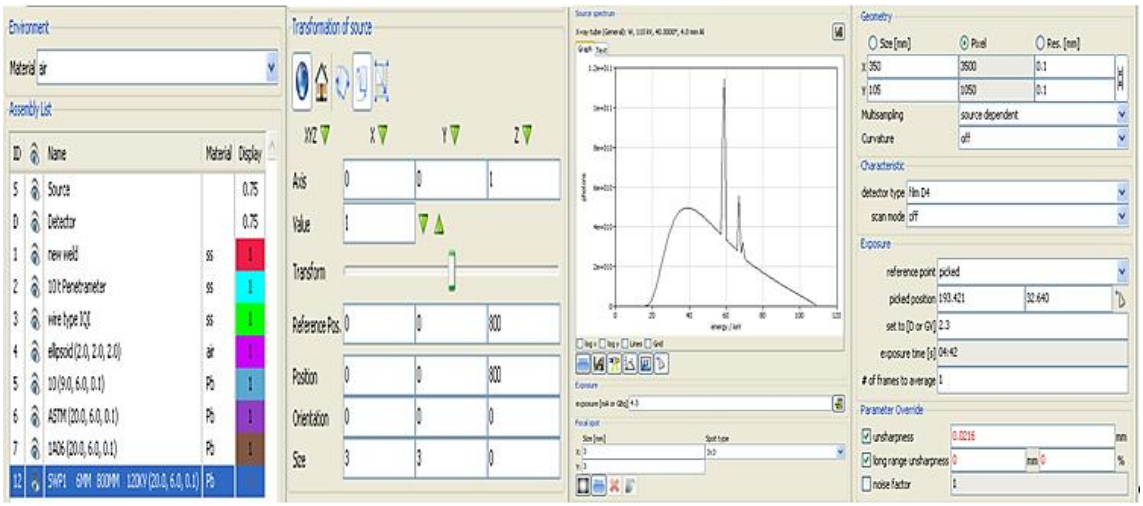

Figure 4. Radiographic testing parameters of weld pad simulation

1.5. Image computing

The last phase of image generation changes over the approaching radiation intensity to the output units of chosen detector. The detector was chosen as radiographic films from the predefined list of radiographic simulator. By default for film radiography, the exposure time is set such that the darkest point in the image has an optical density of 2.5. The darkest point with a density of 2.4 happens to be in the gas pore, while the density in the base material is around 2.3. But if we set optical density as 2.3 using a reference point in the base material, then mean density are 2.3 in the base material, approximately 2.6 in the gas pore and 2.0 in the root. Due to the film grain, the optical density is not perfectly constant but displays small variations. In the wake of setting source and detector parameters the genuine simulation of the exposure was processed. This outcome is relating to synthetic radiograph. The simulation program automatically set the correct exposure time.

1.6. Simulation flow chart for radiographic testing

Typical flow chart for the simulation is shown in below.

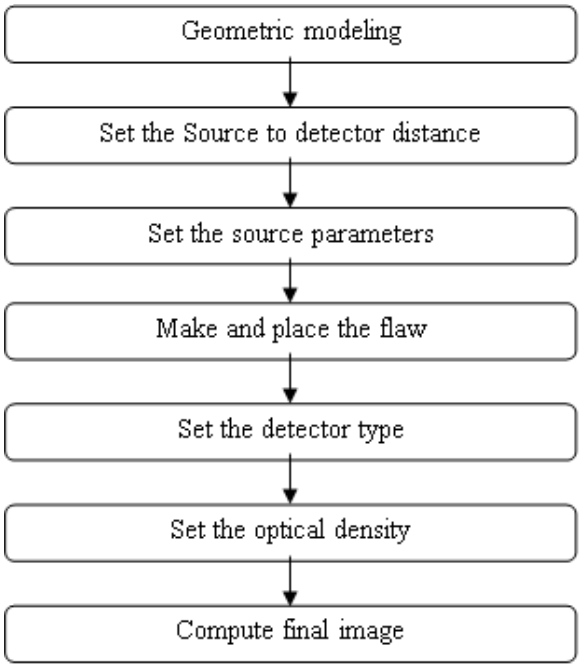

1.7. Radiographic contrast

Radiographic contrast describes the degree of differences between densities of radiograph in two adjacent areas. Contrast will be shading of gray from one extreme to the other. Radiographic contrast depends on two factors. These are subject contrast and film contrast. Figure 5 shows various parameters affecting radiographic contrast.

1.7.1. Subject contrast

It is defined as the ratio of X- ray intensities transmitted through two different areas of a specimen. It depends upon the radiation quality, intensity distribution, and scattered radiation. The higher the radiation energy, the lower would be the subject contrast.

1.7.2. Film contrast

It refers to the slope of characteristic curve of the film at a given density. It depends upon the type of film, processing conditions and optical density. It is independent of radiation quality.

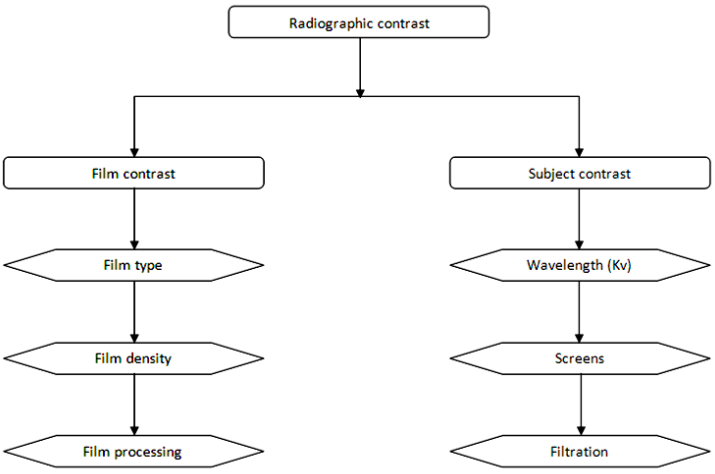

Figure 5. Radiographic contrast affecting parameters

1.8. Geometric unsharpness

Geometric unsharpness is one of the important factors used for assessing quality of radiograph. Sharpness of the image is a component of various elements. In radiographs with poor unsharpness all fine points of interest are recorded blurred. Film with a fine grain size is favored for excellent radiography, being fit for settling fine subtle elements. There is a geometrical unsharpness caused by the finite radiation source, known as the "focal spot". A large diameter source will cause a broad penumbra which implies that the edges of an image become blurred as appeared in Figure 6.

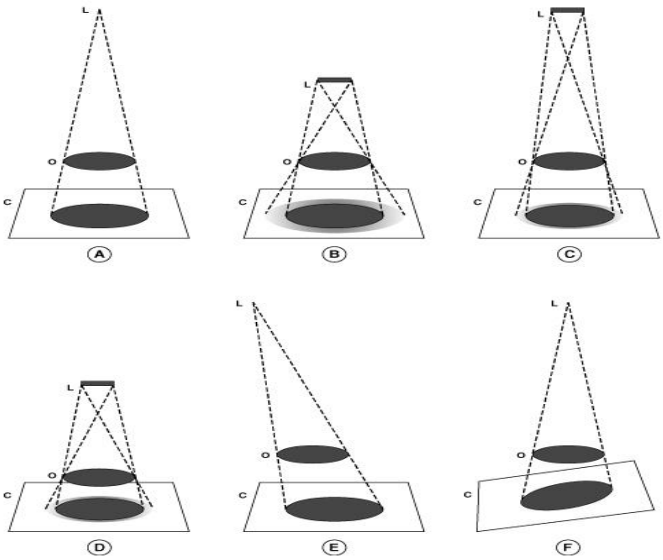

Figure 6. Geometric unsharpness affecting parameters
(L- Source, O-Object, C-Detector)

The farther from the object being radiographed than the more subtle is this impact – tragically the further away the source is from the object then the more is the exposure time – double the distance quadruples the time. To limit the penumbra and increment sharpness the source should be as small as possible, the film should to be as close tothe back of the object as could be expected under the circumstances, the source should be as a long way from the object as could reasonably be expected, remembering the increasing of exposure time, and finally fine grained film should to be utilized [13]. The focal spot size of X-ray should be small, (use point source if possible). See Figure 6, A and C. The source of X-Ray should be as far away as possible from the object. See Figure 6, B and C. The detector should be as close to the object as possible. See Figure 6, B and D. The source should be directly perpendicular to the detector. See Figure 6, A and E. The detector and object planes should be parallel to each other. Compare Figure 6, A and F.

2. Experiment

Photograph of a typical weld sample and experimental setup used for validation of radiographic simulation studies is shown in the Figure 7. Stainless Steel 304L weld sample of 6mm thick with dimension of 100mm X100mm was used for the validation study. The Balteu X-ray unit used for these investigations is with current set at10 mA and maximum voltage of 160 kV. A fine grain medium speed film (Agfa D4) was used. A wire type penetrameter with wire diameters ranging from 80 microns to 250 microns was used. Plate with hole type penetrameter with step number 10 and holes 4T, 2T and 1T was also used. The penetrameters were placed on the source side is expected that both type of penetrameter would be able to indicate that the sensitivity of 2% is achieved. The radiographic parameters used for investigation of the weld pad are given in Table 1.

Table 1. Radiographic parameters employed.

Parameters	Values
Selected Voltage	110kV, 120kV,130kV
Current	4.3mA
Technique employed	Single-wall Single-image
Selected Source to Film distance	1000mm, 800mm, 600mm
Film used	Agfa D4
Penetrameter	Wire type(ASTM 1A06) and Hole type(10T)
Processing conditions	Manual, Standard
Density on radiograph	2.20 - 2.37
Sensitivity achieved	4%

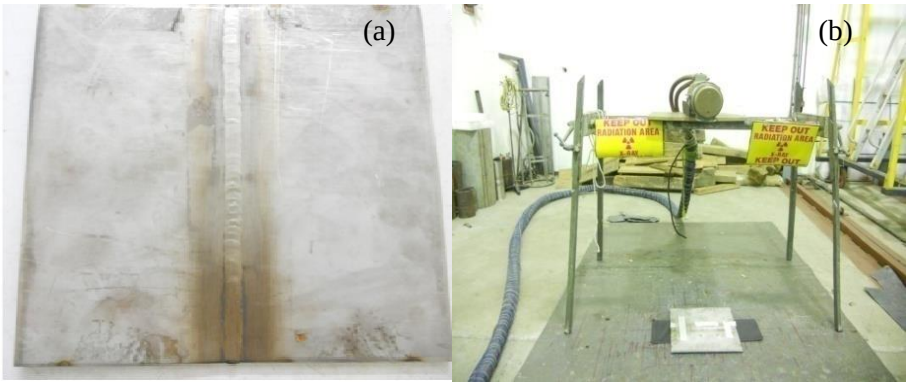

Figure 7. 6mm thick SS 304L plate TIG welded (a) and experimental setup of radiographic testing (b)

3. Results

3.1. Optical density variation

The exposure time derived from the radiographic simulation with the optical density (OD) at base material as 2.3 was used for the experimental validation. For exposure time obtained from simulation the optical density achieved in experimental study is listed for various tube voltages and source to film distance. The table also tabulates the error percentage. Optical density value for simulation, i.e. 2.3.Experiment values are shown in Table 2.

Table 2. Error percentage between experiment and simulation of optical density.

Voltage	130kV		120kV		110kV	
SFD	EXP	Error%	EXP	Error%	EXP	Error%
1000mm	2.34	+1.71	2.28	-0.87	2.21	-3.91
800mm	2.24	-2.61	2.37	+3.04	2.25	-2.17
600mm	2.35	+2.17	2.24	-2.61	2.20	-4.35

3.2. Geometrical unsharpness variation

Apart from the radiographic inspection simulation for optimization of parameters, a study was carried out on the influence of geometric unsharpness in defect sizing. Defect size valuation was carried out for the geometric unsharpness varying from 0.01 to 0.3. Table 3 shows the variation in defect size of 2mm porosity with geometric unsharpness ranging from 0.01 to 0.3. Line profile across the porosity (size 2mm) for geometric unsharpness 0.01, 0.1, 0.2, 0.3 is plotted in the Figure 8. This Figure clearly reveals

that the variation in defect size is minimum for geometric unsharpness of 0.01 and it keeps increasing with increase in geometric unsharpness.

Table 3. Effect of geometric unsharpness on the defect sizing

Ug (mm)	Defect size (mm)
0.01	2.01
0.05	2.05
0.10	2.10
0.15	2.14
0.20	2.18
0.25	2.20
0.30	2.23

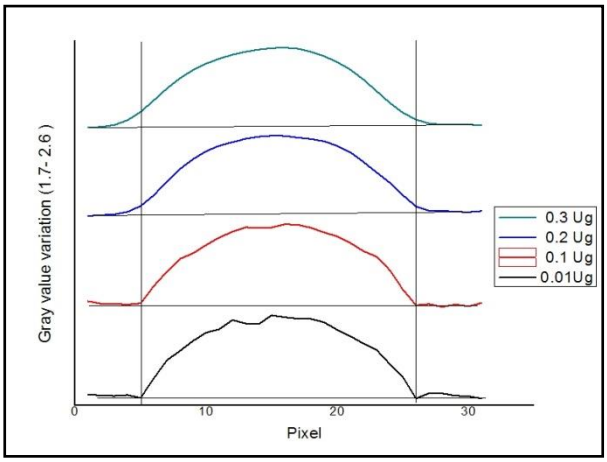

Figure 8. The line profile across the porosity with actual size of 2mm for varying geometric unsharpness

3.3. Film contrast variation

Final radiographic images were obtained by varying the source to film distance, voltage and with varying film grains for constant optical density value of 2.3. Figure 9 shows the contrast of the image obtained at different voltages. The film contrast values were computed from the radiographic images and the values are presented in Table 4.

The simulated radiographic images obtained at various tube voltages reveal the variation in the film contrast achieved and role of it in defect detection. Figure 10 shows the line profile analysis of weld in *IMAGEJ* software.

Table 4. Film contrast achieved with three possible source to film distance and tube voltage

SFD (mm)	Voltage (kV)		
	130	120	110
1000	0.42	0.52	0.62
800	0.48	0.56	0.64
600	0.50	0.58	0.69

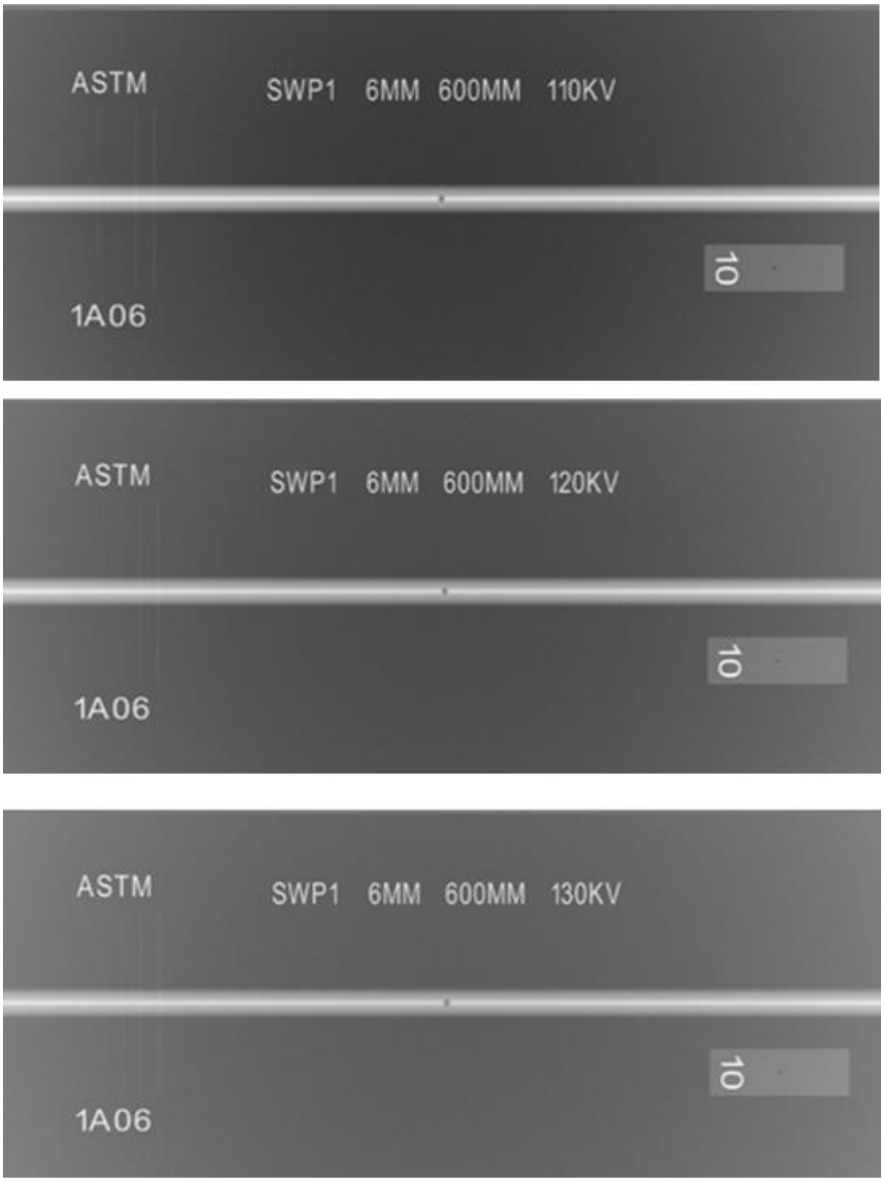

Figure 9. The synthetic radiographs of the weld pad at various tube voltage

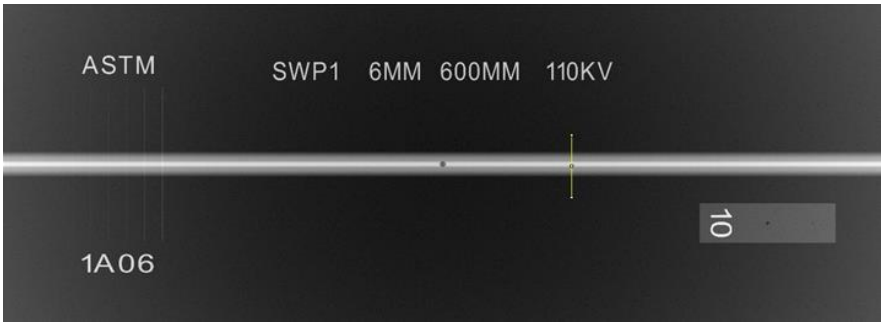

Figure 10. Analysis of the film in *IMAGEJ* software

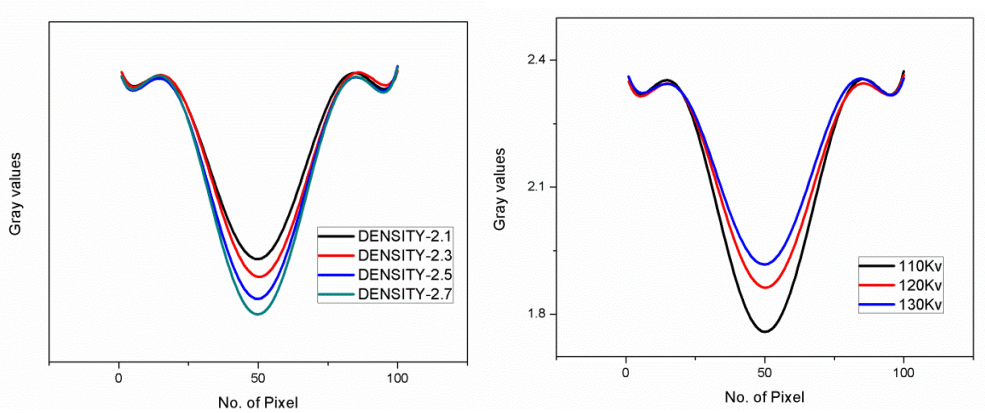

Figure 11. Contrast variation at different optical density and different voltages

Figure 11 shows contrast variation of different optical densities. SFD 600mm and D4 film are used in this arrangement for optical density value range from 2.1 to 2.7 and voltage value range from 110 kV to 130 kV. The Figure shows that high optical density give a higher contrast. Figure 11 shows gray value variation of the film along the line profile of the weld. It shows low voltage gives the high contrast. Figure 12 shows the contrast variation for different films. Here D4, D5, D7 films were used with similar SFD (600mm) and Optical density (2.3). The results clearly shows that D4 film gives the good contrast than other films.

The output of the entire process is simulated radiograph which intently coordinates experimental images. The ensuing utilization of quantitative models brings about reasonable images and coordinating exposure times.

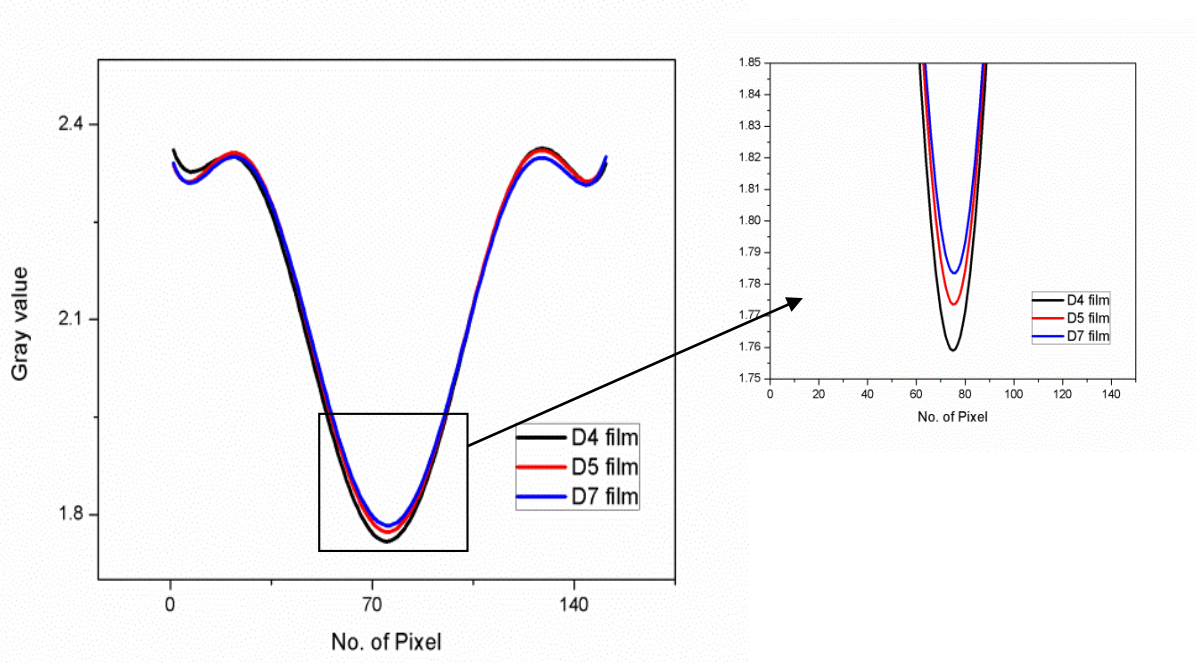

Figure 12. Contrast variation for different films (a); enlarged image showing the differences in gray values for its corresponding No. of Pixel

4. Conclusions

Simulation of radiographic examination has been carried out using *artist* software. Radiographic simulation studies were carried out to determine the optimum tube voltage, source to film distance, film density, and type of film for standard weld pad with similar configuration of the tanks. The modeling

results were validated with experimental work carried out on weld pad sample of 6mm thickness. The optimum parameters obtained from the simulation for optical density of 2.3 were used for carrying out the radiographic examination of the weld pad. The optical density within range of 2.20-2.37 for different tube voltage and source to film distance were obtained in the experimental work. The error percentage in the optical density achieved by experimental radiographic inspection was ± 5% of the simulation. Hence, the optimization parameters using simulation for the weld pad helps in eliminating the over exposure & under exposure shots of the experiment, reduce inspection time and increase defect detectability of the inspection.

References

[1]. J.Kodandaraman, B.M.AnandaRao, K.Rajan, Shekhar Kumar, N.K.Pandey, A.Ravisankar, 2017, "Concurrent Trends in Indian Fast Reactor Fuel Reprocessing", International Conference on Fast Reactors and Related Fuel Cycles, Yekaterinburg, Russian Federation

[2]. Ravisankar, A., V. Vijayakumar, BM AnandaRao, U. KamachiMudali, V. Sundararaman, and R. Natarajan., 2013, "An Indian Perspective of the Development of Fast Reactor Fuel Reprocessing Technology." in International conference on Fast Reactors and related Fuel Cycles: Safe Technologies and Sustainable Scenarios FR13, Paper no. TN-CN-199/256, 4-7.

[3]. Natarajan, R., V. Vijayakumar, RV SubbaRao, and N. K. Pandey, 2015, "Experiences of Reprocessing of Plutonium-rich Mixed Carbide Fuels", *Journal of Radio analytical and Nuclear Chemistry*, **304**, 401-407.

[4]. R. Halmshaw,1987, "*Non Destructive Testing*", Edward Arnold, London, ISBN 13: 9780713136340.

[5]. Tillack, G-R., C. Bellon, and C. Nockemann., 1995, "Computer simulation of radiographic process-a study of complex component and defect geometry", review of progress in QNDE, **14A**, 665-672.

[6]. Bellon, Carsten, et al. , 1997, "Computer simulation of X-ray NDE process coupled with CAD interface." *Review of Progress in Quantitative Nondestructive Evaluation*. Springer US, 325-330.

[7]. Tillack, G-R., Christina Nockemann, and CarstenBellon. 2000, "X-ray modeling for industrial applications." NDT & E International, **33(7)**, 481-488.

[8]. Elshafiey, I., and J. N. Gray, 1996, "Optimization Tool for X-Ray Radiography NDE" ,*Journal Quantitative Nondestructive Evaluation*, **15**, 425-432.

[9]. Bellon, Carsten, and Gerd-RüdigerJaenisch, 2008, "aRTist – Analytical RT Inspection Simulation Tool for Industrial Application" In Proceedings of 17th World Conference on Nondestructive Testing, Shanghai, China.

[10]. Bellon, Carsten, Andreas Deresch, Christian Gollwitzer, and Gerd-RüdigerJaenisch., 2012, "Radiographic Simulator aRTist: Version 2." in Proceedings of 18th World Conference on Nondestructive Testing, Durban, South Africa.

[11]. Bellon, Carsten, 1997, "Computer simulation of X-ray NDE process coupled with CAD interface." Review of Progress in Quantitative Nondestructive Evaluation. Springer, Boston, MA, 325-330.

[12]. Bellon, Carsten, Andreas Deresch, and Gerd-RüdigerJaenisch., 2015, "Radiography Simulation with aRTist–Combining Analytical and Monte Carlo Methods." in Proceedings of International Symposium on Digital Industrial Radiology and Computed Tomography, Ghent, Belgium.

[13]. Raj B, Venkataraman B, 2004, "*Practical radiography*", Alpha Science Int'l Ltd, *ISBN 13: 9781842651889.*